

PAPER • OPEN ACCESS

A Python based automated tracking routine for myosin II filaments

To cite this article: L S Mosby *et al* 2020 *J. Phys. D: Appl. Phys.* **53** 304002

View the [article online](#) for updates and enhancements.





IOP | ebooks™

Bringing together innovative digital publishing with leading authors from the global scientific community.

Start exploring the collection—download the first chapter of every title for free.

A Python based automated tracking routine for myosin II filaments

L S Mosby^{1,2}, M Polin^{1,2}  and D V Köster¹ 

¹ Centre for Mechanochemical Cell Biology, University of Warwick, Coventry CV4 7AL, United Kingdom

² Physics Department, University of Warwick, Coventry CV4 7AL, United Kingdom

E-mail: d.koester@warwick.ac.uk and m.polin@warwick.ac.uk

Received 29 January 2020, revised 26 March 2020

Accepted for publication 8 April 2020

Published 27 May 2020



Abstract

The study of motor protein dynamics within cytoskeletal networks is of high interest to physicists and biologists to understand how the dynamics and properties of individual motors lead to cooperative effects and control of overall network behaviour. Here, we report a method to detect and track muscle myosin II filaments within an actin network tethered to supported lipid bilayers. Based on the characteristic shape of myosin II filaments, this automated tracking routine allowed us to follow the position and orientation of myosin II filaments over time, and to reliably classify their dynamics into segments of diffusive and processive motion based on the analysis of displacements and angular changes between time steps. This automated, high throughput method will allow scientists to efficiently analyse motor dynamics in different conditions, and will grant access to more detailed information than provided by common tracking methods, without any need for time consuming manual tracking or generation of kymographs.

Keywords: single particle tracking, automated detection, myosin

(Some figures may appear in colour only in the online journal)

1. Introduction

Molecular motors are important for many cellular processes such as cell cortex dynamics, cell migration, and the intracellular transport of vesicles. Purification of various molecular motors from tissue samples or after recombinant expression, and the analysis of their biochemical and bio-physical properties in reconstituted systems, was instrumental in furthering our understanding of the motors and how they are regulated in live cells. Whereas most molecular motors operate individually or in dimers, myosin II—a 520 kDa protein consisting of two head domains, two light chains and two heavy chains that make up the tail [1] - usually forms filaments from about 10 (non-muscle myosin II) [2] up to 200–600 (muscle myosin II) [3] proteins at physiological salt conditions. This gives rise

to cooperative effects between the myosin head domains that govern the effective binding dynamics, speed and processivity of these myosin II protein ensembles.

Briefly, myosin II is an ATPase with a low binding affinity for filamentous actin when bound to ATP. Once bound to actin, myosin II undergoes a conformational change upon hydrolysis of its associated ATP, resulting in a power stroke that propels the motor towards the barbed end of the actin filament. After release of the free phosphate (Pi), the remaining ADP is exchanged with ATP, causing the detachment of the myosin II head domain from the actin filament [1, 4]. As a result, the interactions of myosin II head domains with actin filaments depend on the ATP concentration. Within a myosin II filament, the multiple head domains give rise to cooperative effects which have been studied theoretically [4–6], and recent advances in microscopy and the design of reconstituted acto-myosin networks have allowed the study of individual myosin II filaments experimentally [7, 8].

Traditionally, motor dynamics were studied indirectly using motility assays [9, 10], optical tweezers [11, 12],



Original Content from this work may be used under the terms of the [Creative Commons Attribution 4.0 licence](https://creativecommons.org/licenses/by/4.0/). Any further distribution of this work must maintain attribution to the author(s) and the title of the work, journal citation and DOI.

kymograph analysis [7, 13, 14], or common single particle tracking (SPT) routines that identify point-like structures [15, 16]. These methods have drawbacks, for example kymographs only track dynamics along a given path in one dimension. This is adequate for tracking motor dynamics along fixed, straight tracks, but can be a limiting factor for tracking particles in dynamic networks where many events occur within the field of view and paths can change over time. An additional drawback is the loss of spatial data (only motion along one dimension is analysed as a function of time), hence this method cannot be used to study two-dimensional diffusive motion. SPT routines that are commonly used to study videos of biological molecule dynamics with low signal to noise ratios (such as ImageJ TrackMate, <https://imagej.net/TrackMate>, or Particle Tracker, <https://mosaic.mpi-cbg.de/MosaicToolboxSuite/ParticleTracker.html>) cannot be used to study particle orientation as they fit signals with Gaussian intensity profiles in order to obtain the localisation of usually resolution limited particles. However, the orientation of myosin II filaments is a valuable parameter that can be used to characterise their dynamics more precisely and to distinguish between their different modes of motion. In this case either random, diffusive motion or directed, processive motion is expected to occur depending on the number of myosin head domains interacting with actin filaments [4–6].

Here, we modified an image analysis routine from Astrophysics used to recognize galaxies [17–19] to automatically detect myosin II filaments, as both types of object are characterised by their elongated, elliptical shapes with limited signal to noise ratios in large, heterogeneous data sets. After particle detection, tracks are generated by comparing the positions, orientations and detected areas of particles between subsequent frames. We developed this routine to analyse data for muscle myosin II filament dynamics in a flat, lipid anchored actin filament network [8]. This Python based routine worked robustly in the detection of myosin II filaments in a dynamic and changing actin network, and made it possible to generate tracks of hundreds of myosin II filaments split into regions of diffusive and processive motion. This tracking routine that we have called myoSPT (code can be found at <https://github.com/cmcb-warwick/myoSPT>) could have wider applications in the tracking of other anisotropic objects such as actin filaments or bacteria, and could be used to characterise their motion after taking into account orientational fluctuations.

2. Methods

2.1. Experimental data

A detailed description of the experimental setup and data used in this work can be found in [8]. Briefly, interferometric scattering (iSCAT) microscopy [20] was used to visualise myosin II filament dynamics within a thin actin filament network tethered to a supported lipid bilayer. Actin filaments and skeletal myosin II filaments were purified from chicken breast muscle following established protocols. Glass cover slips (#1.5 borosilicate, Menzel, Germany) were cleaned in

a sequence of 2% Hellmanex (Hellma Analytics, Mühlheim, Germany) followed by thorough rinses with EtOH and MilliQ water, and were blow dried with N₂ before being used for the preparation of experimental chambers. After formation of supported lipid bilayers (containing 98% DOPC and 2% DGS-NTA(Ni²⁺) lipids (Avanti Polar Lipids Inc. US)) and addition of our actin-membrane linker protein HKE (decahistidine-ezrin actin binding domain), polymerized actin filaments and myosin II filaments were incubated in KMEH (50 mM KCl, 2 mM MgCl₂, 1 mM EGTA, 20 mM HEPES, pH 7.2) to allow the formation of membrane tethered acto-myosin networks [8, 21]. Images were recorded on an iSCAT microscope setup equipped with a CMOS camera and processed to reflect interferometric contrast values in 32 bit with a pixel size of $0.034 \times 0.034 \mu\text{m}^2$.

At the onset of experiments ($t = 1$ min) myosin II filaments were added to the membrane bound actin filament network in the presence of 100 μM ATP (referred to in the following as highest [ATP]). Myosin II filament dynamics were followed at an effective frame rate of 5 Hz for 20 minutes, during which the ATP concentration decreased steadily. At approximately $t = 16$ min the acto-myosin networks became contractile, corresponding to ATP concentrations $< 10 \mu\text{M}$ ATP (referred to as lowest [ATP]) [8, 21].

2.2. Myosin II filament detection

We used the Python programming language as a platform for the myosin II filament tracking method based on the Python library for source extraction and photometry (SEP) [17–19], which generates the position, spatial extent, and orientation of elliptical particles for each frame of a time lapse image sequence. To distinguish individual myosin II filaments, we first applied a signal and area threshold to isolate probable myosin II filament detections from background, followed by the application of a refined area threshold to distinguish individual myosin II filaments from aggregates and to reduce the rate of false-positive detection due to poor signal to noise ratios. For the first step, a detection was defined as a region of > 40 pixels, each with an intensity of at least $1.5\sigma_{\text{g,rms}}$ above the local background intensity, where $\sigma_{\text{g,rms}}$ is the global root-mean-square error of the spatially varying background of the image. These minimum area and intensity cutoffs allowed confident detection of myosin II filaments without falsely detecting background fluctuations.

The SEP Python package computes a set of ellipse parameters (a : semi-major axis, b : semi-minor axis, θ : orientation on a $-\pi/2 \leq \theta \leq \pi/2$ domain) for each detection based on the spatial dispersion of its intensity profile (sections 10.1.5 and 6 of v2.13 of the S Extractor User's Manual by E. Bertin). The area of each detection was then calculated as $A = \pi ab$ (figures 1(a) and (b)). For clarity the ellipse parameters were scaled to $x = 6x_{\text{detected}}$ ($x = a$ or b) to allow for better representation of the detected object by eye [19]. These scaled values will be used throughout as the parameter estimates for the ellipses. It should also be noted that the observed signal is a result of the convolution between the real signal and the point-spread

function of the microscope. For these reasons the areas calculated using this method have only been used for diagnostics.

In order to prevent the false-positive detection of background intensity fluctuations (figure 1(c)) a minimum area cutoff was implemented. After considering the probability distribution function of the detected myosin II filament areas for a sample data set with a high signal to noise ratio, the minimum area cutoff was defined as equal to the smallest detected area $A_{\min} = 0.151 \mu\text{m}^2$. An average area for a single myosin II filament detection was also calculated as $A_{\text{av}} = 1.25A_{\text{mode}}$, where A_{mode} was the maximum value of an exponentially-modified Gaussian distribution of the form [22],

$$G(A; A_0, \lambda, \sigma, C_1, C_2) = C_1 \left(\frac{\lambda}{2} \right) e^{\left(\frac{\lambda}{2} \right) [2(A_0 - A) + \lambda \sigma^2]} \text{erfc} \left(\frac{A_0 - A + \lambda \sigma^2}{\sqrt{2}\sigma} \right) + C_2, \quad (1)$$

fitted to the area probability distribution function of a data set recorded at high ATP concentration that displayed minimal myosin II filament aggregate formation (figures 1(a) and (b)). Here A is the area of the detected feature, and $A_0, \lambda, \sigma,$ and $C_{1,2}$ are parameters to be fitted. The distribution in equation (1) was fitted as an empirical method of quantifying A_{av} . At lower ATP concentrations the sample data sets contained many myosin II filament aggregates (figure 1(d)), which resulted in a higher than expected rate of detection of large area values contributing to the exponentially decaying tail of the area distribution shown in figures 1(a) and (b). In order to observe the dynamics of single myosin II filaments, tracks including larger aggregates must be removed before analysis.

2.3. Myosin II filament tracking

Tracks of myosin II filament motion were generated by considering the spatial displacement and the change in area of the detected particle between subsequent frames. First, it was checked whether the change in position of a detection between two consecutive frames was suitably small. An estimation of the maximum bound velocity of a myosin II filament of $v_{\text{max}} \sim 0.6 \mu\text{m s}^{-1}$ suggests filaments can move a maximum distance of $|\Delta \mathbf{x}|_{\text{max}} \sim 4$ pxl between frames. Here, the magnitude of the change in position between frames was limited to $|\Delta \mathbf{x}| = \sqrt{(\bar{x}_2 - \bar{x}_1)^2 + (\bar{y}_2 - \bar{y}_1)^2} \leq 6$ pxl for a new detection to be considered part of an existing track (where \bar{x}, \bar{y} are the co-ordinates of the centroid of the detected particle, and the subscripts indicate initial (1) and final (2) positions), to allow for small deviations in position and shape.

Second, a detection at time t_2 was also only added to the track of a detection at time t_1 if its area $A(t_2)$ satisfied $A(t_1) - A_{\text{av}} \leq A(t_2) \leq A(t_1) + A_{\text{av}}$, which allowed for the transient overlap of two detections. This can lead to tracks being cut into multiple shorter tracks due to overlap events, which tends to skew dwell time and total displacement distributions towards lower values, in particular in data sets with lots of aggregation or clustering of particles. For this work the dwell time of a myosin II filament was defined as the amount of time it was observed for, which is strongly related to the time

it spent bound to the underlying actin network. In order to minimise the effects of noise on dwell time measurements, only detections associated with tracks observed for at least two frames are included for the remaining area analysis. As a result of the implemented intensity and area thresholds, it can be assumed that the detected particles must have been bound for the majority of the exposure time (here 200 ms).

In order to derive an appropriate maximum area threshold that minimises the detection of myosin II filament aggregates, the effect of varying the maximum area (as a multiple of the average area, A_{av}) on average system variables was analysed (figures 2(a) and (b)). The maximum area was set to $A_{\text{max}} = 4A_{\text{av}} = 3.251 \mu\text{m}^2$ as it maximised the measured average dwell time, while also being larger than the value that maximised the measured average distance travelled. It should be noted that all tracks that contain a point with an area $A > A_{\text{max}}$ have been removed in their entirety from the data to be analysed in order to prevent artificially skewing the dwell time and displacement distributions. In order to measure dwell times and total displacements as accurately as possible, only tracks that ended (by detachment or by leaving the field of view) by the end of the video were included in the analysis. The effect of myosin II filaments leaving the field of view on the measured dwell time was found to be negligible, as less than 4% of tracks ended within 6 pxl (the maximum allowed filament displacement between time steps) of the edge of the video. The final probability distribution function describing the detected areas after applying the above corrections is shown in figures 2(c) and (d).

When two myosin II filaments transiently overlapped, the aggregate was always appended to the track with the current longest dwell time in order to probe longer track dynamics. The ratio of tracks that ended within $l = \sqrt{A_{\text{av}}}$ of any point on another track (potentially due to aggregation) was independent of the dwell time of the tracks (results not shown). Similarly, the dwell time distributions and associated characteristic timescales, including the average dwell time, of the tracked myosin II filaments at varying ATP concentrations did not change significantly after the removal of the tracks that ended in an overlap event (results not shown). These results suggest that the overlap events do not introduce a characteristic timescale into the dwell time analysis, and hence can be ignored.

Following particle detection and tracking, analysis is carried out as follows:

Tracks that contain large displacements that could be due to processive particle motion are located (section 2.4),

Processive regions of tracks are isolated using bounds on the time-correlation of the filament displacements (section 2.4),

Filament orientation is analysed to complete the parameterisation of each track (section 2.5).

Following these steps, distributions can be derived for myosin II filament displacements, mean-squared displacements, orientations, mean-squared angular displacements, and

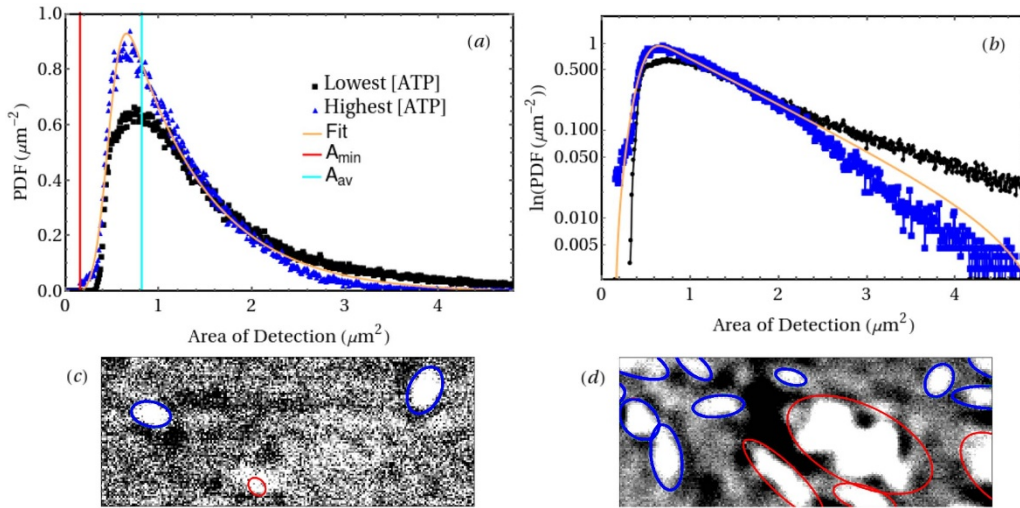


Figure 1. (a) Probability distribution functions of detection areas for the sample data sets with the highest (blue) and lowest (black) ATP concentrations, corresponding to the time points $t = 1$ min, and $t = 16$ min of the experiment, respectively. Decreasing the ATP concentration increases the rate of overlap events between myosin II filaments, leading to aggregation and a higher proportion of the population in the exponentially decaying tail of the distribution. All detections with areas less than the minimum area cutoff A_{\min} (red vertical line, equal to the minimum area detection in the high signal-to-noise ratio data set with the lowest ATP concentration) were removed from all data sets. An exponentially-modified Gaussian distribution was fitted to the highest ATP concentration data (orange) to find the average area $A_{\text{av}} = 1.25A_{\text{mode}}$ (cyan vertical line), where A_{mode} is the area corresponding to the maximum of the fitted distribution. (b) Semi-logarithmic plots of the distributions showing their decay profiles. Both distributions exhibit a Gaussian distribution at small areas and an exponentially decaying tail at larger areas. (c) Example of anomalously small area detection in the data set with the highest ATP concentration (red) due to poor signal to noise ratio and a disperse region of pixels with intensity greater than $1.5\sigma_{\text{g,rms}}$ above the local background intensity. Detections with areas $A_{\min} \leq A \leq A_{\max}$ are included for comparison (blue). (d) Examples of myosin II filament aggregates in the data set with the lowest ATP concentration (red).

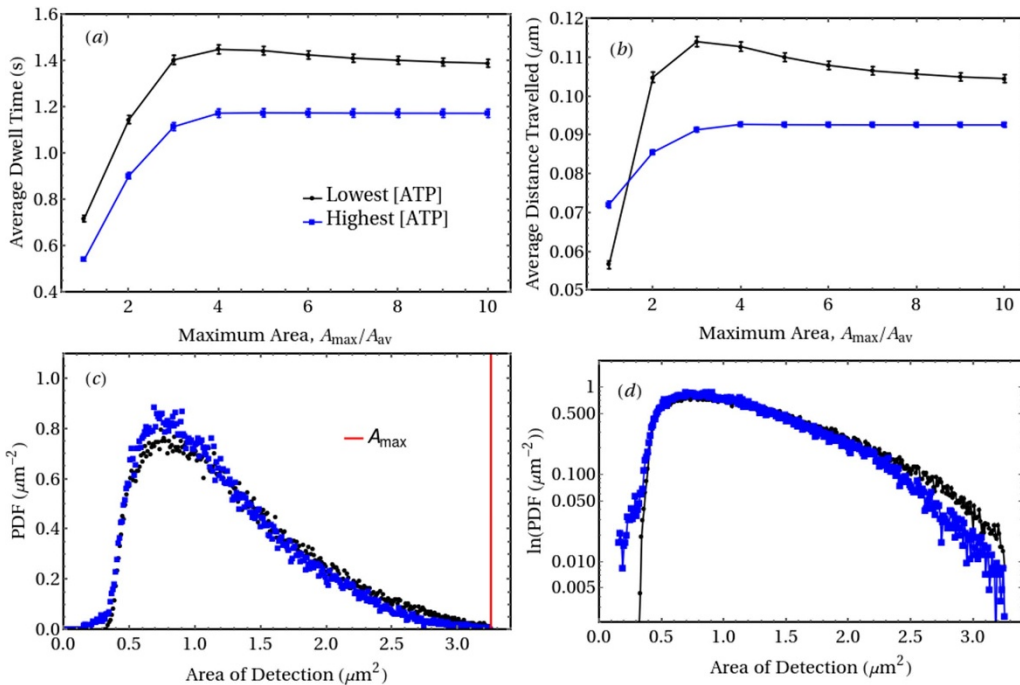


Figure 2. (a) The effect of varying the maximum area cutoff A_{\max} (in multiples of A_{av}) on the average dwell time of the myosin II filaments in the iSCAT videos for the highest (blue) and lowest (black) ATP concentration data sets, corresponding to the time points $t = 1$ min, and $t = 16$ min of the experiment, respectively. (b) The effect of varying the maximum area cutoff A_{\max} on the average straight-line distance the myosin II filaments travelled between their initial and final positions in the iSCAT videos. (c) The corrected probability distribution functions of detection areas after the application of the derived minimum and maximum area cutoffs. Red vertical line shows the maximum area cutoff. (d) Semi-logarithmic plots of the corrected area distributions that have the form of a Gaussian distribution at small areas and an exponentially decaying tail at larger areas. After the removal of tracks containing large area detections, the exponential tail of the distributions decays to zero at A_{\max} .

dwell times, along entire tracks and separately along regions of purely processive motion.

2.4. Defining processive regions of myosin II filament tracks

Of particular interest in this work is the splitting of tracks into regions of processive (directed) motion and diffusive (non-directed) motion. The processive motion of the myosin II filaments executed when the filaments are fully bound to the underlying actin network has a much longer persistence length than the diffusive motion exhibited by the filaments when they are only partially bound to the surface. Tracks were defined as being diffusive or processive using the formalism from the work by Jeanneret *et al* [23]; firstly tracks that contain large, directional displacements that cannot be a result of Brownian motion were identified, and then the exact frames corresponding to these displacements were isolated by considering the correlation in the displacements between adjacent time steps.

A purely diffusive, spherical particle with a time-dependent position $\mathbf{x}(t)$ and diffusivity D in two-dimensions will always have an average displacement of zero and a mean-squared displacement equal to $\langle \Delta \mathbf{x}(t)^2 \rangle_D = 4Dt$. Assuming that the myosin II filaments being tracked exhibit non-diffusive motion, this expectation value can be used as a lower bound of the mean-squared displacement required to identify a particle as moving processively. We note that, in principle, a filament could exhibit $\langle \Delta \mathbf{x}(t) \rangle \neq 0$ and therefore a larger value of $\langle \Delta \mathbf{x}(t)^2 \rangle$, due to hydrodynamic interactions with nearby processive filaments. Although here we do not consider these potential events, they do not seem to be relevant in our experiments.

Due to the anisotropy in the shape of the ellipsoidal myosin II filaments, it is expected that they will exhibit different diffusivities in the directions parallel (D_a) and perpendicular (D_b) to their orientation (or semi-major axis). This means that, when in the diffusive state, a filament will move with an average diffusivity $D_{avg} = (D_a + D_b)/2$ in the lab frame (which is the quantity measured in this work), but that the individual, directional diffusivities along the x and y axes in the lab frame (D_x and D_y respectively) will only tend to the value D_{avg} at long times [24]. The analytical form of the diffusion tensor for an ellipse shows that D_x and D_y are functions of the initial orientation of the ellipse, and decay monotonically towards the average diffusivity D_{avg} with the timescale [24],

$$\tau_D = \frac{1}{4D_\theta}, \quad (2)$$

where the angular diffusivity D_θ implicitly includes information about the average eccentricity of the myosin II filaments. This is by definition the timescale for the diffusion tensor to become isotropic.

Neglecting any single frame detections, the average dwell time of the myosin II filaments at the lowest ATP concentration (corresponding to the longest average dwell time) was $\langle t \rangle = (1.449 \pm 0.019)$ s after considering 15647 detected filaments. The angular diffusivity was calculated from the gradient of a linear fit to the first ten points, 2 s, of the mean-squared

angular displacement data when plotted against time, and for this data set was $D_\theta = (0.077 \pm 0.003)$ rad² s⁻¹. This corresponds to an angular decorrelation time of $\tau_D = (3.27 \pm 0.10)$ s. The measured angular diffusivity was higher for the data set at the highest ATP concentration, as on average fewer processive regions of track were detected that have high correlation in their orientations. In this case $\tau_D = (1.39 \pm 0.07)$ s, which is more comparable to the average dwell time for the data set $\langle t \rangle = (1.173 \pm 0.018)$ s after considering 14016 detected filaments.

As $\tau_D > \langle t \rangle$ for all sample data sets, individual filament trajectories will maintain a good degree of correlation with their initial direction along their full length, and the diffusivities D_x and D_y along the lab frame axes for individual filament trajectories will be different from the long-term average diffusivity D_{avg} . However, their average, $(D_x + D_y)/2$, provides an unbiased estimate of D_{avg} even for individual trajectories [24]. In this work, we sample a large population of trajectories whose initial orientations are isotropically distributed in the lab frame. In this case, even the single-axis diffusivities D_x and D_y are equal to D_{avg} when the average over the whole set of trajectories is considered. The average diffusivity that we report, $\langle (D_x + D_y)/2 \rangle$, is averaged over the ensemble of all recorded trajectories, and is an unbiased estimate of D_{avg} .

Tracks with processive regions were isolated by requiring the mean-squared displacement of a myosin II filament to be greater than $16D_{avg}\Delta t (= 4\langle \Delta \mathbf{x}(t)^2 \rangle_{D_{avg}})$ over a period of $\Delta t = 2$ s at some point along the track. This sets the requirement that a filament must have a dwell time of at least 2 s to be defined as moving processively, but as processive motion has been connected to stronger binding to the actin network and longer dwell times [8], we believe this threshold to be reasonable. The value of the diffusivity D_{avg} used to recognise processive tracks was derived from the sample data set with the highest ATP concentration (using the same method as for the value of D_θ above and accounting for the 2D system), in order to minimise the effects of processive motion on the measurement. It has been assumed that the average filament diffusivity is independent of ATP concentration. The effect of processivity on the measured (translational) diffusivity and angular diffusivity for each of the sample data sets is shown in figure 3. The value of the diffusivity used to recognise processive tracks was $D_{avg} = (0.00048 \pm 0.00004)$ $\mu\text{m}^2 \text{s}^{-1}$, resulting in a threshold for processivity of $16D_{avg}\Delta t \sim 0.015$ μm^2 .

Once a track with a region of large displacement was identified, the points that corresponded to the processive motion were isolated by considering the correlation in displacements between adjacent time steps [23]. For a diffusive process this correlation is $\langle d\mathbf{r}_{t+\Delta t} \cdot d\mathbf{r}_t \rangle = 0$ (where $d\mathbf{r}_t = \mathbf{r}(t + \Delta t) - \mathbf{r}(t)$), and the variance in this quantity is

$$\text{Var}(d\mathbf{r}_{t+\Delta t} \cdot d\mathbf{r}_t) = 8D_{avg}^2\Delta t^2, \quad (3)$$

after averaging over all possible initial orientations. This means that the standard deviation in the scalar product $d\mathbf{r}_{t+\Delta t} \cdot d\mathbf{r}_t$ is $\sigma(d\mathbf{r}_{t+\Delta t} \cdot d\mathbf{r}_t) = 2\sqrt{2}D_{avg}\Delta t$, even for a spatially anisotropic particle. Although this could be used as a threshold to

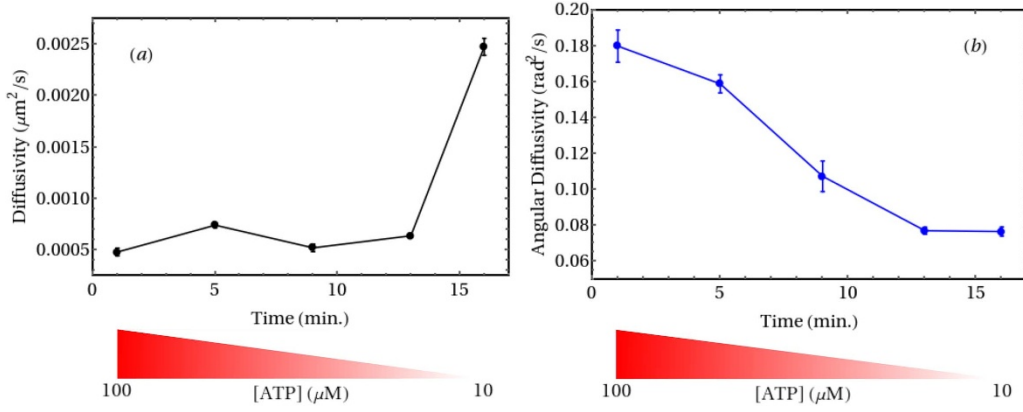


Figure 3. (a) Dependence of myosin II filament (translational) diffusivity on the time since the start of the experiment from which the sample data sets were collected, with $[ATP] = 100 \mu\text{M}$ at $t = 1$ min and $[ATP] < 10 \mu\text{M}$ at $t = 16$ min. As the ATP concentration decreases, the filaments move further on average from their initial position as a function of time as the fraction of time that filaments spend moving processively increases. This leads to an increased observed average diffusivity. (b) Dependence of filament angular diffusivity on the time since the start of the experiment, with $[ATP] = 100 \mu\text{M}$ at $t = 1$ min and $[ATP] < 10 \mu\text{M}$ at $t = 16$ min. As the fraction of time that the filaments spend moving processively increases, the width of the distribution describing the difference between their orientation and direction of propagation decreases, resulting in a decrease in the observed angular diffusivity.

identify the sections of the track that could be deemed processive, it would still be subject to a significant number of false-positives. To circumvent this problem, we followed the work by Jeanneret *et al* [23] and focused instead on the average signal

$$C_t^+ = \frac{\mathbf{dr}_{t+2\Delta t} \cdot \mathbf{dr}_{t+\Delta t} + \mathbf{dr}_{t+\Delta t} \cdot \mathbf{dr}_t}{2}. \quad (4)$$

A myosin II filament was defined as moving processively at time t if $C_t^+ > 2\sqrt{2}D_{avg}\Delta t$. Similarly, because the decision of whether or not a filament was moving processively at time t should be invariant under time reversal symmetry, for each point on the track the averaged correlation C_t was calculated for both directions in time. Time inversion generated a new form of equation (4) to be calculated,

$$C_t^- = \frac{\mathbf{dr}_{t-2\Delta t} \cdot \mathbf{dr}_{t-\Delta t} + \mathbf{dr}_{t-\Delta t} \cdot \mathbf{dr}_t}{2}, \quad (5)$$

but for a purely diffusive particle the value to compare this to would be invariant under this transformation, $\sigma(\mathbf{dr}_{t-\Delta t} \cdot \mathbf{dr}_t) = 2\sqrt{2}D_{avg}\Delta t$. An example of a track that has been split into diffusive and processive regions is shown in figure 4.

Using the average correlation in both directions in time to define whether a myosin II filament was moving processively ensured that points on a filament's track at the edge of a processive region were not neglected incorrectly (for example C_t^+ cannot be defined for the final three points of any track), and that short (≤ 3 time step) deviations from processive motion between two processive regions of track were still classified as processive. For example, if a myosin II filament exhibited a single, sharp jump in its propagation direction, and hence processivity, this could be the result of the filament binding to a new actin filament and continuing its processive motion. In this case it would be correct to define this as a single processive region. This method could artificially increase the timescales of observed processive regions by small amounts,

but has been used to minimise the impacts of small deviations in filament processivity, such as the artificial splitting of processive regions, and to track edge effects. In this work the added requirement that a point is only defined as processive if it is in a region of at least five similarly defined processive points (over a time of 1 s) is used. A binary signal b_t has been defined such that $b_t = 1$ at time t if either $C_t^\pm > 2\sqrt{2}D_{avg}\Delta t$, and $b_t = 0$ otherwise, as shown in figure 4(c).

2.5. Interpreting myosin II filament orientation

The SEP Python package generates the orientation angles of each elliptical particle it detects in an image (above the threshold area and intensity described in section 2.2) on a $-\pi/2 \leq \theta \leq \pi/2$ domain. The myosin II filaments studied in this work break the expected symmetry along the semi-major axis of an ellipse by having a preferential direction of propagation when bound to actin, and so their orientation must be defined on a $-\pi \leq \theta \leq \pi$ domain instead. Extending this domain further and tracking filament orientation on the domain $-\infty < \theta < \infty$ ensures that no large jumps are observed in filament orientation due to the periodic boundaries of a $-\pi \leq \theta \leq \pi$ domain. This re-parameterisation is especially important for the calculation of angular diffusivity.

Of the two possible initial orientation angles (parallel and anti-parallel to the semi-major axis of the elliptical myosin II filament detection), it was assumed that the correct choice would minimise the time average of the difference between the filament's orientation at time t , θ_t , and propagation direction at time t , $\phi_t = \arctan((\bar{y}_{t+\Delta t} - \bar{y}_t)/(\bar{x}_{t+\Delta t} - \bar{x}_t))$ (where \bar{x}_t, \bar{y}_t are the co-ordinates of the centroid of the detected ellipse at time t). This average was calculated over either the processive region(s) of track, or the entire track if the filament exhibited purely diffusive motion. It has been found that filaments moving processively have a smaller average value of $\phi_t - \bar{\theta}_t$ (where $\bar{\theta}_t = (\theta_{t+\Delta t} + \theta_t)/2$) [8], with examples shown

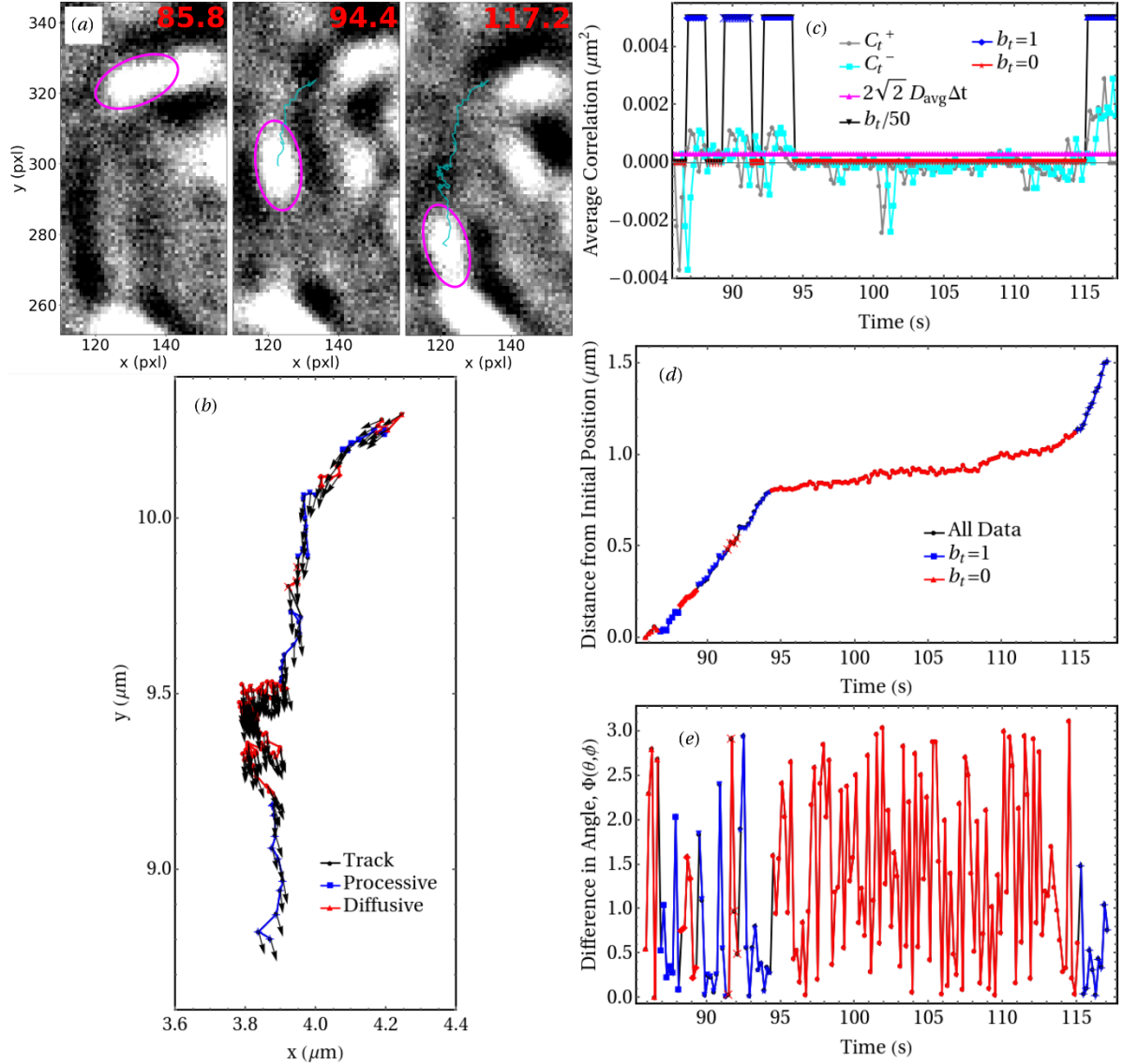


Figure 4. (a) Snapshots from the iSCAT video with the lowest ATP concentration showing track of detected myosin II filament (cyan) with elliptical filament shape (magenta), labeled by time since the start of the video in seconds. (b) Track of example myosin II filament split into processive (blue) and diffusive (red) regions. Arrows show filament orientation at each time. (c) Parameters used to define whether a point on the track is processive or diffusive. Regions where either C_t^+ or C_t^- (equations (4) and (5)) are greater than $2\sqrt{2}D_{avg}\Delta t$ for at least five frames are processive, and $b_t = 1$. (d) Distance from initial position increases approximately linearly in processive regions, but plateaus in long diffusive region. (e) Difference between orientation angle and direction of propagation (calculated from equation (8)) appears to have more frequent fluctuations with larger amplitudes in the diffusive regions.

in figure 5, so using processive region(s) to derive the filament’s initial orientation would be preferable.

Once a detection is added to a track, it was assigned the orientation angle that minimises the filament’s change in orientation between frames, either parallel or anti-parallel to its semi-major axis. This assumes that a filament cannot rotate by more than $|\Delta\theta_{max}| = \pi/2$ between successive frames. Unwrapping the angle θ by keeping track of the number of complete rotations allowed us to track a filament’s orientation on a $-\infty < \theta < \infty$ domain. It has also been assumed that the propagation direction of a filament cannot vary by more than $|\Delta\phi_{max}| = \pi$ between frames, so the new propagation direction minimised the change in the directions between frames taking into

account the 2π periodicity of the domain. Of the two possible orientation tracks in angle-space that resulted from the two available initial filament orientations, the selected path is the one that maximised the sum

$$\Psi(\theta, \phi, T) = \sum_{i=0}^{(T/\Delta t)-1} \cos(\phi_{i\Delta t} - \bar{\theta}_{i\Delta t}), \quad (6)$$

where T was the total duration of the iSCAT video being analysed (with corresponding time between frames Δt). If the filament exhibited processive motion, then the sum in equation (6) was instead taken from $i = T_s/\Delta t$ to $i = (T_f/\Delta t) - 1$, where T_s and T_f were the start and finish times of the processive

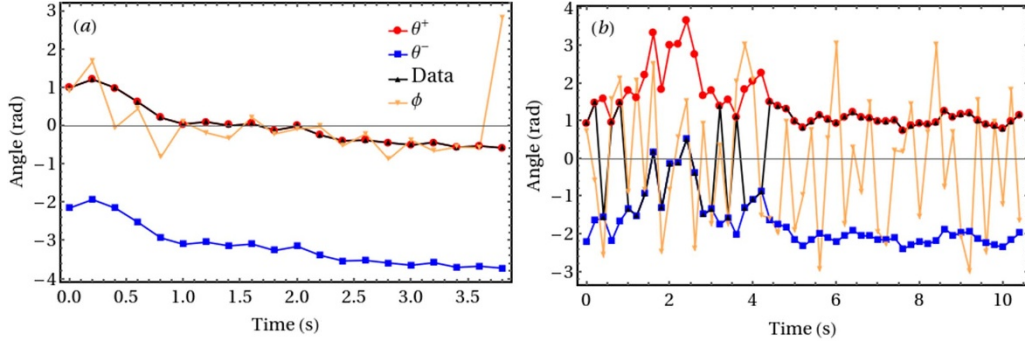


Figure 5. Different angular track properties for single tracks. (a) Purely processive track, propagation direction ϕ is aligned with orientation angle θ^+ for majority of track. Black data shows the orientation extracted by the SEP Python package, red and blue data represent possible orientation tracks in angle-space, θ^+ and θ^- respectively. The θ^+ data maximises the sum in equation (6). (b) Purely diffusive track, propagation direction ϕ varies faster and with greater amplitude than orientation angle θ^\pm . Orientations extracted by the SEP Python package are split amongst both of the possible orientation tracks in angle-space.

region(s). The cosine term inside the sum was a maximum when the average filament orientation was aligned with its propagation direction, and was a minimum when the directions were anti-parallel, and implicitly took into account the 2π periodicity of the domain. The values $\Psi^\pm(\theta_t^\pm, \phi_t, T)$ corresponding to the two possible orientation paths θ_t^\pm (labelled as one path will always start with a positive orientation angle and the other a negative one) will always be separated by a factor of -1 , as,

$$\Psi^\pm(\theta^\pm, \phi, T) = \cos(\pi) \Psi^\mp(\theta^\mp, \phi, T) = -\Psi^\mp(\theta^\mp, \phi, T), \quad (7)$$

so only one path needed to be followed in order to choose the correct initial orientation.

By exploiting the domain of the arccos function from the Math Python package, the magnitude of the difference between the orientation angle and the direction of propagation could be calculated at each time t as

$$\Phi(\bar{\theta}_t, \phi_t) = |\arccos(\cos(\phi_t - \bar{\theta}_t))|. \quad (8)$$

Using equation (8), the distance moved by a myosin II filament at each time, $|\Delta \mathbf{x}_t| = r_t$, could then be separated into components parallel, $|\Delta \mathbf{x}_t|_{\text{para}} = r_t |\cos(\Phi(\bar{\theta}_t, \phi_t))|$, and perpendicular, $|\Delta \mathbf{x}_t|_{\text{perp}} = r_t |\sin(\Phi(\bar{\theta}_t, \phi_t))|$, to the filament orientation. This could be used for example to estimate the elements of the (effective) diffusivity tensor during diffusive motion, or to assess correlations between processive displacements and myosin orientation.

Finally, the error in individual orientation measurements due to image pixelisation and inherent pixel noise could be estimated by using the tracking procedure presented here to analyse particles permanently stuck to a surface.

Using the results of this angle tracking, a histogram of $\bar{\theta}_t - \bar{\theta}_0$ could be plotted for each time t after the initial observation of a filament. These results showed that the orientation distribution evolved as a Gaussian with width proportional to time $\sim D_\theta t$ (results not shown), which justified *a posteriori* the use of a linear fit to calculate the angular diffusivity from the mean-squared angular displacements.

3. Discussion

The computational methods described here were developed with the aim of analysing the motion of myosin II filaments containing multiple motor protein domains when bound to an underlying actin filament network. Regular point or circular body tracking algorithms could not be used to accurately parameterise the motion of the elongated, ellipsoidal myosin II filaments, and would not be able to provide any information about their angular fluctuations. Splitting tracks into regions of diffusive or processive motion allows us to potentially probe the dynamics of different bound states for the myosin II filaments, which could be extended to the study of different biological systems. Following the development and calibration of the SPT method outlined in this paper, analysis of the full myosin II filament data set has yielded interesting information about the dwell time distribution and spatial dynamics of bound myosin II filaments as a function of the ATP concentration of the system [8].

The current method did not take into account the depth of the sample in which the myosin II filaments move, such that only shapes in the x-y plane are analysed without considering the dynamics along the optical axis. Even though myosin II filaments leaving the x-y plane would display altered detection areas, this effect was neglected in this work due to the underlying lipid membrane tethered actin network constituting a quasi-two-dimensional system with a thickness of 2–6 actin filaments (i.e. < 100 nm). More generally, it would be possible to use the particle detection routine outlined in this work to detect three dimensional ellipsoids when data from multiple z-planes are combined, and to then use the same methods to minimise false-positive detections and to generate particle tracks. As a result of our code being written in the open programming language Python, it is expected that other groups will be able to easily adapt it for future applications. This novel SPT routine (code can be found at <https://github.com/cmcb-warwick/myoSPT>) can be used to study the dynamics of particles at varying length-scales, and has potential applications in the fields of fluorescence and light microscopy.

Acknowledgments

D V K acknowledges the Kukura lab (University of Oxford) for enabling the imaging of myosin II filament dynamics on their iSCAT microscopes. D V K thanks the Warwick-Wellcome QBP for funding (RMRCB0058). L M and M P gratefully acknowledge support from Leverhulme Trust Grant RPG-2016-260.

ORCID iDs

M Polin  <https://orcid.org/0000-0002-0623-3046>

D V Köster  <https://orcid.org/0000-0001-8530-5476>

References

- [1] Spudich J A 2014 Hypertrophic and dilated cardiomyopathy: Four decades of basic research on muscle lead to potential therapeutic approaches to these devastating genetic diseases *Biophys. J.* **106** 1236–49
- [2] Billington N, Wang A, Mao J, Adelstein R S and Sellers J R 2013 Characterization of three full-length human nonmuscle myosin II paralogs *J. Biol. Chem.* **288** 33398–410
- [3] Thoresen T, Lenz M and Gardel M L 2013 Thick filament length and isoform composition determine self-organized contractile units in actomyosin bundles *Biophys. J.* **104** 655–65
- [4] Erdmann T and Schwarz U S 2012. Stochastic force generation by small ensembles of myosin II motors *Phys. Rev. Lett.* **108** 188101
- [5] Erdmann T, Bartelheimer K and Schwarz U S 2016 Sensitivity of small myosin II ensembles from different isoforms to mechanical load and ATP concentration *Phys. Rev. E.* **94** 052403
- [6] Stam S, Alberts J, Gardel M L and Munro E 2015 Isoforms confer characteristic force generation and mechanosensation by myosin II filaments *Biophys. J.* **108** 1997–2006
- [7] Melli L, Billington N, Sun S A, Bird J E, Nagy A, Friedman T B, Takagi Y and Sellers J R 2018 Bipolar filaments of human nonmuscle myosin 2-A and 2-B have distinct motile and mechanical properties *eLife* **7** 32871
- [8] Mosby L S, Hundt N, Young G, Fineberg A, Polin M, Mayor S, Kukura P and Köster D V 2020 Myosin II filament dynamics in actin networks revealed with interferometric scattering microscopy *Biophys. J.* **118** 1946–57
- [9] Homsher E, Wang F and Sellers J R 1992 Factors affecting movement of F-actin filaments propelled by skeletal muscle heavy meromyosin *Am. J. Physiol.-Cell Physiol.* **262** C714–23
- [10] Kron S J and J a Spudich 1986 Fluorescent actin filaments move on myosin fixed to a glass surface *Proc. Natl Acad. Sci. USA* **83** 6272–6
- [11] Veigel C, Wang F, Bartoo M L, Sellers J R and Molloy J E 2002 The gated gait of the processive molecular motor, myosin V *Nat. Cell Biol.* **4** 59–65
- [12] Rock R S, Rice S E, Wells A L, Purcell T J, Spudich J A and Sweeney H L 2001 Myosin VI is a processive motor with a large step size *Proc. Natl Acad. Sci. USA* **98** 13655–9
- [13] Grover R, Fischer J, Schwarz F W, Walter W J, Schwille P and Diez S 2016 Transport efficiency of membrane-anchored kinesin-1 motors depends on motor density and diffusivity *Proc. Natl. Acad. Sci.* **113** E7185–93
- [14] Bieling P, Telley I A, Piehler J and Surrey T 2008 Processive kinesins require loose mechanical coupling for efficient collective motility *EMBO Rep.* **9** 1121–7
- [15] Pierobon P, Achouri S, Courty S, Dunn A R, Spudich J a, Dahan M and Cappello G 2009 Velocity, processivity and individual steps of single myosin V molecules in live cells *Biophys. J.* **96** 4268–75
- [16] Andrecka J, Arroyo J O, Takagi Y, de Wit G, Fineberg A, MacKinnon L, Young G, Sellers J R and Kukura P 2015 Structural dynamics of myosin 5 during processive motion revealed by interferometric scattering microscopy *Elife* **2015** 1–15
- [17] Bertin E and Arnouts S 1996 SExtractor: Software for source extraction *Astron. Astrophys. Suppl. Ser.* **117** 393–404
- [18] Barbary K 2016 SEP: Source Extractor as a library *J. Open Source Softw.* **1** 58
- [19] Barbary K 2018. SEP Documentation Release 1.0.3. (<https://buildmedia.readthedocs.org/media/pdf/sep/latest/sep.pdf>)
- [20] Young G *et al* 2018 Quantitative mass imaging of single biological macromolecules *Science* **360** 423–7
- [21] Köster D V, Husain K, Iljazi E, Bhat A, Bieling P, Mullins D R, Rao M and Mayor S 2016 Actomyosin dynamics drive local membrane component organization in an in vitro active composite layer *Proc. Natl Acad. Sci. USA* **113** E1645–54
- [22] Golubev A 2010 Exponentially modified Gaussian (EMG) relevance to distributions related to cell proliferation and differentiation *J. Theor. Biol.* **262** 257–66
- [23] Jeanneret R, Pushkin D O, Kantsler V and Polin M 2016 Entrainment dominates the interaction of microalgae with micron-sized objects *Nat. Comm.* **7** 12518
- [24] Han Y, Alsayed A M, Nobili M, Zhang J, Lubensky T C and Yodh A G 2006 Brownian motion of an ellipsoid *Science* **314** 626–30